IEEE Access
Multidisciplinary | Rapid Review | Open Access Journal

Received 31 December 2022, accepted 16 January 2023, date of publication 6 February 2023, date of current version 13 February 2023.

Digital Object Identifier 10.1109/ACCESS.2023.3243060

RESEARCH ARTICLE

Inductor-Aid Step-Up LLC Resonant Wireless Power Transfer

KIN LUNG JERRY KAN AND KA WAI ERIC CHENG, (Fellow, IEEE)
Power Electronics Research Center, The Hong Kong Polytechnic University, Hong Kong

Corresponding author: Ka Wai Eric Cheng (eric-cheng.cheng@polyu.edu.hk)

This work was supported in part by the University Grant Council General Research Fund (GRF) Hong Kong under Grant PolyU 152218/19E.

ABSTRACT An inductor-aid step-up LLC wireless power transfer (WPT) system is proposed in this paper. It could step up the WPT output voltage beyond the conventional LLC series-series (SS) compensation method. Employing a parallel inductor with the transmitter coil to lessen the circuit impedance thus the inverter exhibits a new gain curve. The constant frequency operation and simple control of two series active switches in the parallel inductor branch shows a practical improvement of conventional constant frequency LLC WPT system, in terms of voltage demand, new standards and applications. Even the frequency modulation LLC WPT system could be benefited from this enhanced topology rather than to deteriorate the inverter current stress and unnecessary over-rating of magnetic components. The receiver side compensation tank has no additional voltage drop and overcurrent. A 300W prototype has been constructed to validate the concept and performed at 90% efficiency.

INDEX TERMS Wireless power transfer (WPT), LLC, resonant converter, fundamental harmonic approximation (FHA) method.

I. INTRODUCTION

WPT system evolution happens from theories to applications and standards that facilitate human lives [1], [2]. Static and dynamic electric vehicle (EV) chargers, ball-joint structure WPT systems, implantable bioelectronics, and oil pipe have been proposed, and the research covers furious electrical, magnetic, and structural analysis [3], [4], [5], [6], [7]. Integration of the WPT system and the communication system, and the information security system were well illustrated in [8]. The WPT system could be achieved by laser, radiofrequency, microwaves, inductive, and magnetic resonant wireless that is focused in this paper for the high efficiency and low reactive power [9]. The compensation capacitors were deployed to resonate with the leakage inductances in the transmitter (Tx) and Receiver (Rx) sides so that the circuit could perform at high efficiency. There are three main compensation networks to eliminate the reactive power in the WPT system: LCL, LCC, and LLC methods. LCL performs high efficiency along with the whole load range. However, the Rx side reactance and resistance would be reflected to the Tx side as well as the large size [10]. LCC needs one more resonant inductor and capacitor component in the circuit. Besides, in WPT applications, even be regardless of the consideration of the Rx side load factor, zero current switchings (ZCS) would be hard to achieve without the auxiliary circuit. The complex resonance tank makes it hard to maintain the circuit stabilization when the magnetic linkage disturbance occurs [11]. LLC SS compensation method features high parameter tolerance and voltage source transfer function with no reflected secondary reactance [12]. High tolerance to misalignment and zero voltage switching (ZVS) has drawn many researchers to spread the study area. In circuit design, the practical requirement might constrain the resonant tank selection. To achieve the desired WPT system, the equivalent conversion of the third-order, fourth-order, LLC, LCC, and LCC resonant tank was investigated in [13].

Many LLC circuit analysis methodologies raised in the past, covered the circuit gain analysis derivation from the conduction angle of rectifier diode, Lagrandian dynamics

The associate editor coordinating the review of this manuscript and approving it for publication was Alon Kuperman.

model analysis, modified fundamental harmonic approximation (FHA), and the time-domain simplified equations with iterative calculation model [14], [15], [16], [17]. Among them, the FHA is straightforward and accurate enough to conduct the LLC design by the comparison of FHA and frequency domain analysis with time-domain partial or complete correction and the operation mode-based analysis presented in [18]. It concluded that the accuracy of FHA is higher when the system operates under a low-quality factor and near the compensated resonant frequency. FHA has been widely examined and used in many applications, including the closed-loop control converter, bidirectional DC-DC converter, wide output vehicle chargers with power factor correction, and waterproof vessel wireless charger due to the high accuracy, simple design process, and control strategy [19], [20], [21], [22], [23]. Many subtle control methods, such as the closed-loop design and the frequency doubler method to raise the output power based on FHA have been investigated in LLC non-WPT system area [24], [25]. A 3.3kW with 97.6% efficiency LLC design was built in [26]. This paper elaborates on the LLC circuit loss analysis comprehensively and boosts the topology efficiency by magnetizing current optimization. However, the magnetic component is not feasible for WPT application as the wide switching frequency interval from 48.4kHz to 86.2kHz is inapplicable. In a WPT system, decreasing the switching frequency may boost the output voltage but results in a large magnetizing current. A 1-MW SS WPT system has been developed for a train [27]. The configuration comprises one Tx and 4 parallel placing Rx. The 5 cm air gap brings an extremely low coupling coefficient of about 0.05, whereas the induction voltage on both sides should be no more than 10kV. However, It is a constant frequency supply with only one output voltage level. The reason is the WPT circuit gain curve would be too sharp to deliver a stable performance by frequency modulation. Reference [28] presents a fixed phase shift method to control the conversion ratio, but its quality factor value makes it impractical to the WPT system. The proposed circuit of this paper would provide another higher voltage level without the frequency control.

Magnetics design is important in the WPT system. Some interesting application is induction heating – a classical wireless power, a 12kW induction wok, and the cordless ironing system were presented in [29] and [30], respectively. In this paper, the WPT magnetic component will be designed as the single Tx with the vertical flux type to expand the applications. In the Tx coils, even a distribution dynamic WPT system could be considered as a static situation when the moving velocity is far lower than the switching frequency [31]. Vertical flux type WPT system proved to have a higher tolerance of misalignment and shortened the magnetic flux equivalent length so that the reluctance drops. Supplying by one turn Tx coil and 26 cm air gap, 80% efficiency 100kW LLC SS WPT system was conducted. The only drawback is fixed frequency and voltage gain of the output side [32]. Integrated magnetic winding design decreases the magnetizing current with the cancellation of leakage flux [33]. However, the reluctance estimation of the WPT system could be sophisticated. The variable series inductance of the LLC resonant tank changes the circuit resonant frequencies to meet the closed-loop control [34]. It also raises the requirement of Tx and Rx communication and the high voltage saturation risk of the variable inductor.

This paper proposes the inductor-aid method to step up the output voltage with the constant frequency operation. Add two more active switches and one parallel inductor could provide a promising high step-up level of output voltage, which could contribute to the higher utility of the LLC WPT system. In section II, the foundation of the LLC WPT would be introduced to illustrate the circuit basis. The difference between the WPT and non-WPT applications will be addressed. In section III, steady-state analysis of the proposed circuit, including the electric and magnetic parameters, would be elaborated in the circuit gain analysis, operation principle, ZVS, and losses analysis. Section IV provides the proposed inductor-aid step-up LLC WPT design framework, procedure and simulation results. A comparison of the conventional LLC and the proposed method will be conducted in this section and the next. Section V is the experimental verification and benchmarking. A 300W prototype has been developed with 90% efficiency. This paper examines all the circuit hardware parameters and testing results. The comparison works exhibit the proposed circuit states at the overwhelming higher step-up voltage ratio and the lower resonant current than the conventional LLC frequency modulation method. The last section is the conclusion.

II. LLC WPT SYSTEM FUNDAMENTALS

Fig.1 depicts the conventional LLC WPT configuration. Transmitter has a full-bridge inverter with a resonant tank and a magnetic field-generating coil. The duty ratio of the inverter switching devices is 0.5. S_1, S_3 would be ON and OFF concurrently and S_2, S_4 vice versa. f_{sw} is the inverter switching frequency. L_1 is the transmitter coil self-inductance

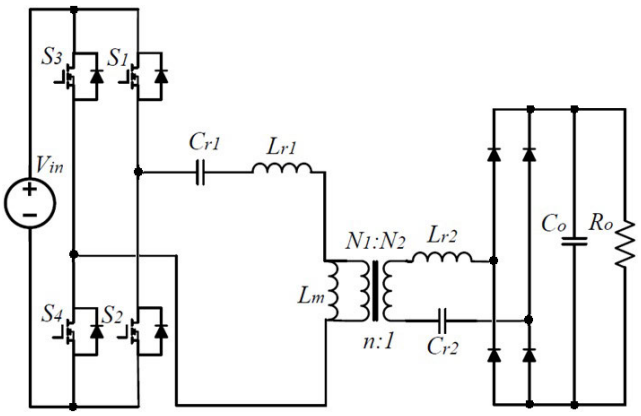

FIGURE 1. Conventional LLC WPT circuit diagram.

that consists of the magnetizing inductance L_m and primary leakage inductance L_{r1}. L_m is the magnetizing inductance of a transformer while the L_{r1} is a dedicated resonant inductance which constitutes the resonant tank with C_{r1} to achieve the frequency modulation in non-WPT applications.

Equations (1) to (4) present the inductance equations and their coupling. However, due to the large reluctance R_m, which comes from the air gap, a coupling coefficient k and mutual inductance M_{12} between the transmitter side and receiver side is low. (3) reveals a considerable portion of leakage inductance occurs in the coil under the loose connection between N_1 and N_2 windings which is high that would be thus utilized as resonant inductance [27], [29]. L_{r2} is the leakage inductance at the Rx side and C_{r2} is the corresponding compensation capacitor.

$$k = M_{12}/\sqrt{L_1 L_2} \tag{1}$$
$$L_m = M_{12}N_1/N_2 \tag{2}$$
$$L_{r1} = L_1 - L_m = L_1 - N_1^2/R_m \tag{3}$$
$$L_{r2} = L_2 - M_{12}N_2/N_1 \tag{4}$$

As mentioned, the air gap constituting the magnetic field transmission path generates a high portion of leakage inductance on both sides; compensation capacitors could be deployed to degenerate the reactance power. There are parallel and series compensation methods on two sides, thus total 4 compensation combinations. Reference [12] validates the series-series compensation that has no reflected Rx side reactance to the primary side at the resonant frequency, and the output characteristics could be considered as the voltage source after the rectifier, which makes it more competitive with the other three compensation combinations. H-bridge modulates the steady DC voltage to the AC square waveform. After that, C_{r1}, L_{r1} and L_m compose the resonant tank in which the current magnetizes the transmission medium and establishes the alternative magnetic field. Magnetic field density B_{m} couples with the receiver coil and core to feed the load. To acquire the steady output voltage under various load conditions, [14] depicts that C_{r1} is designed to compensate L_{r1} and the switching frequency is fixed at the primary resonance frequency $f_{r1} = 1/2\pi\sqrt{L_{r1}C_{r1}}$.

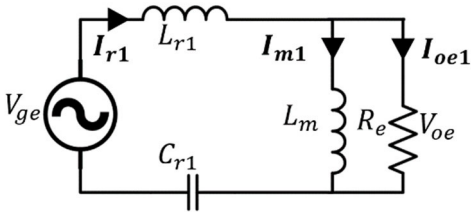

FIGURE 2. FHA simplified circuit.

The first harmonics approximation (FHA) method is effective in streamlining the LLC WPT analysis. It states the simplified circuit as shown in Fig.2. $V_{ge} = 4V_{in}\sin(2\pi f_{sw}t)/\pi$ and $V_{oe} = 4nV_o\sin(2\pi f_{sw}t - \varphi_v)/\pi$ is the fundamental component of input equivalent sinusoidal voltage and output voltage reflected in the primary side respectively. The reflected equivalent resistance load $R_e = 8R_o n^2/\pi^2$. Assume the circuit output voltage $V_o = V_{in}M_g/n$. In a non-WPT LLC system, the inductance ratio L_n of Tx coils could be very large, whereas the air coil LLC WPT system could be small, even less than 1. Circuit resonant current I_r, which conducts in the resonant tank and transmitter coil, composes of the inductive magnetizing current I_m and the output current I_{oe} on the primary side. Therefore, the circuit gain to switching frequency could be derived in (11) and Fig.3. The constant output voltage points that $M_g = 1$ regardless of the load variation occurs when the switching frequency equals the resonance frequency of C_{r1} and L_{r1}. WPT system usually has a small Q_e; thus, the corresponding gain curves would be sharp at the voltage scaling up frequency interval.

$$I_{oe} = \pi I_o(2\pi f_{sw}t - \varphi_v)/2n \tag{5}$$
$$I_m = V_{oe}/j\omega L_m \tag{6}$$
$$I_r = \sqrt{I_m^2 + I_{oe}^2} \tag{7}$$
$$Q_e = \sqrt{L_{r1}/C_{r1}}/R_e \tag{8}$$
$$f_n = f_{sw}/f_{r1} \tag{9}$$
$$L_n = L_m/L_{r1} \tag{10}$$
$$M_g = \left|\frac{jX_{Lm}\|R_e}{(jX_{Lm}\|R_e) + j(X_{Lr} - X_{Cr})}\right| = \left|\frac{L_n f_n^2}{\left[(L_n+1)f_n^2 - 1\right] + j\left[\left(f_n^2 - 1\right)f_n Q_e L_n\right]}\right| \tag{11}$$

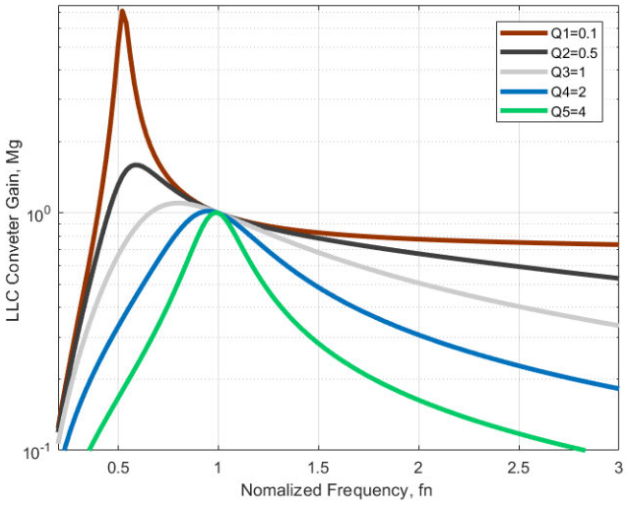

FIGURE 3. LLC frequency response characteristics corresponding to various Q factors by the FHA method.

In order to realize the ZVS of the full-bridge switches, f_{sw} should be set higher than f_{r1}; thus, the circuit would operate inductively. Since the current has a phase lag behind the voltage, when S_2 and S_3 are OFF, I_r still circulates in the primary side. During the dead time, I_r is conducted by the body diode of S_4 and the voltage drop of the active switch is clamped at the diode's forward voltage. It would

sustain even after the switches S_1 and S_4 are ON. Compared with the high input voltage, the diode's forward voltage is usually a comparatively low value; thus, ZVS is achieved. ZVS does reduce not only the switching loss but also lowers the conductive electromagnetic interference.

III. STEADY-STATE ANALYSIS

The proposed inductor-aid step-up LLC topology reveals in Fig.4. LLC WPT system operates at the resonance point and could provide the circuit gain M_{g0} steadily regardless of load variation. In contrast to the conventional LLC WPT system, a higher M_{g1} could be achieved without drawing down the f_{sw}. Assume all internal resistances except the load and voltage drop of diodes are neglected in this section. L_p is the parallel inductor controlled by S_5, S_6. Turning the inductor leg ON means that the inductance of the resonant tank drops, since when L_p conducts, the Tx coil would be parallel connected with an inductor L_p with L_{r1} and L_m. Therefore, the resonant frequency of the LLC inverter circuit rises, and f_{r1} no longer remains at $f_n = 1$ after the switching. The new circuit gain M_{g1} would be higher than before and increase the output voltage at the receiver.

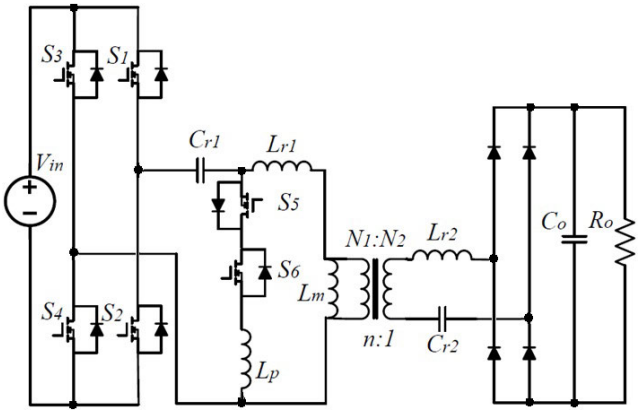

FIGURE 4. FHA proposed constant frequency step-up converter.

A. CIRCUIT GAIN ANALYSIS

Similar to the LLC simplified circuit Fig.2, when S_5 and S_6 are turned ON, the equivalent circuit of the proposed topology is shown in Fig.5 when L_p applies. C_{r1} is the resonant capacitor at the transmitter side. L_m indicates the magnetizing inductance whereas the L_r represents the leakage inductance. The value of these two parameters is decided by the coupling condition of Tx and Rx. The higher k, L_m and lower L_r come with the better coupling condition. Therefore, inserting the high magnetic permeability materials in magnetic components indicates a higher k, the reactive power, induction voltage and energy losses in L_r and L_m could be eased.

Establish the mesh current analysis (12-15) that neglected the Rx side resonant tank. Input current I_{r2} equals the sum of transmitter current I_{tc2} and the reactive current I_{p1}. I_{tc2} is the current that circulates in the transmitter coil, which generates the alternating magnetic field and transfers the active power to the load. The operator "//" means the parallel calculations of the mentioned elements.

$$I_{r2}\left(\frac{1}{j\omega C_{r1}} + j\omega L_{p1}\right) - I_{tc2}j\omega L_{p1} = V_{ge} \tag{12}$$

$$-I_{r2}j\omega L_{p1} + I_{tc2}j\omega\left(L_{p1} + L_{r1} + L_m\right) - I_{oe2}j\omega L_m = 0 \tag{13}$$

$$-I_{tc2}j\omega L_m + I_{oe2}(R_e + j\omega L_m) = 0 \tag{14}$$

$$I_{oe2}R_e = V_{oe2} \tag{15}$$

$$\alpha = 1 + \frac{L_{r1}}{L_p} \tag{16}$$

$$V_{oe2} = \alpha V_{ge} - I_{r2}\frac{L_p + L_{r1} - \omega^2 C_{r1}L_pL_{r1}}{j\omega L_p C_{r1}} \tag{17}$$

$$I_{r2} = V_{ge}/Z_{in} \tag{18}$$

$$Z_{in} = [(R_e//j\omega L_m) + j\omega L_r]//j\omega L_p + 1/j\omega C_r \tag{19}$$

$$I_{tc2} = V_{oe2}/\left(R_e + j\omega L_m\right) \tag{20}$$

$$f_{r2} = \sqrt{\frac{L_P + L_{r1}}{4\pi^2 C_{r1}L_pL_{r1}}} = f_{r1}\sqrt{\alpha} \tag{21}$$

$$V_{o1} = V_{in}/n \tag{22}$$

$$I_{r1} = I_{tc1} = \sqrt{\left(\frac{V_{ge}}{j\omega_0 L_m}\right)^2 + \left(\frac{V_{ge}}{R_e}\right)^2} \tag{23}$$

Switching the f_{sw} to f_{r2} could get to the new resonant operation status. However, the secondary compensation capacitor is designed to resonate with f_{r1}, and capacitor C_{r2} is designed to resonate with L_{r2}. If the primary switching frequency changes, the receiver side would become a capacitive or inductive load and exert the transmitting power.

Fig.5 shows the equivalent circuit with consideration of the secondary resonant tank. According to FHA, the equivalent reflected component of leakage inductance $L_{r2e} = 8L_{r2}n^2/\pi^2$, resonant capacitor $C_{r2e} = C_{r2}\pi^2/8n^2$. $1/(2\pi\sqrt{L_{r2e}C_{r2e}}) = f_{r1}$. Mode 2 has no reflected reactance in primary side. However, when f_{sw} climbs to $f_{r2,}$ the equivalent inductance in the secondary side should be considered.

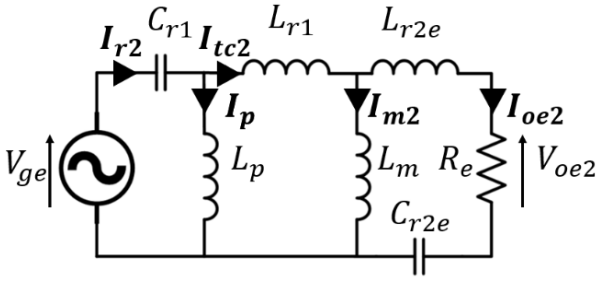

FIGURE 5. Mode 2 FHA simplified circuit of the proposed converter.

The circuit gain M_g with consideration of secondary resonant tank analysis is shown as follows. In Fig.6, the normal lines are the M_g- f_{sw} curve with secondary consideration, while the dashed line is regardless. Apparently, the resonant

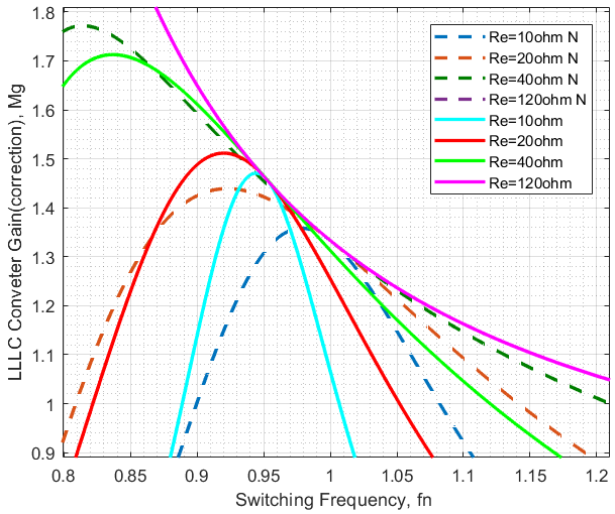

FIGURE 6. Frequency response of Mode 2. Dash lines represent the gain calculation with regardless of secondary compensation network. Full line is the real gain curve.

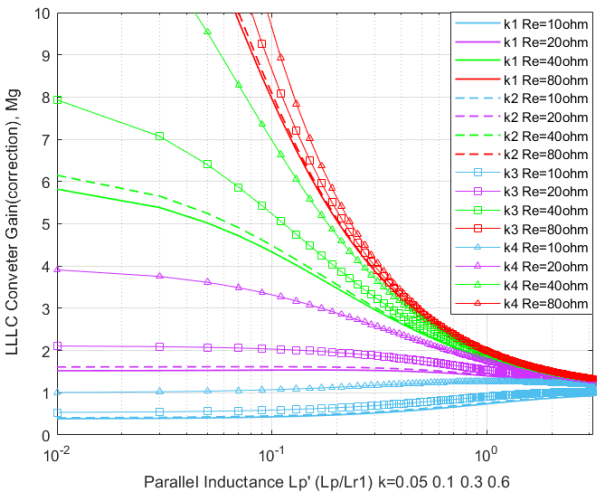

FIGURE 7. Frequency response of nominal L_p value under different output power.

frequency of the circuit with secondary resonant tank consideration f_c is slightly lower than the neglected analysis of (17). Hence, it ensures the inductive operation and ZVS of primary inverter switches. On the other hand, a drop of M_g comes with it. The new circuit gain is M_{gp}. Fig.7 illustrates M_g swags comparatively at the resonant frequency point f_{r2}. The under-voltage problem would be even worst in heavy load conditions.

$$Z_{in} = \frac{1}{j\omega C_{r1}} + j\omega L_p // \left[j\omega L_{r1} + j\omega L_m // \left(R_e + j\omega L_{r2e} + \frac{1}{j\omega C_{r2e}} \right) \right] \tag{24}$$

$$Z_s = R_e + j\omega L_{r2e} + \frac{1}{j\omega C_{r2e}} \tag{25}$$

$$M_{gp} = \frac{R_e}{Z_s} \cdot \frac{Z_s // j\omega L_m}{j\omega L_{r1} + (Z_s // j\omega L_m)} \cdot \frac{Z_{in} - \frac{1}{j\omega C_{r1}}}{Z_{in}} \tag{26}$$

$$V_{o2} = V_{in} M_{gp} / n \tag{27}$$

$$I_{tc2} = \sqrt{I_{m2}^2 + I_{oe2}^2} = \sqrt{\left(\frac{V_{oe2}}{j\omega L_m}\right)^2 + \left(\frac{V_{oe2}}{R_e}\right)^2} \tag{28}$$

$$I_p = \left[I_{tc1} j\omega_2 L_{r1} + \alpha V_{ge} \right] / j\omega_2 L_p \tag{29}$$

B. OPERATIONAL PRINCIPLE

There are two modes of operation through the switching of S_5 and S_6, as shown below:

Mode 1: When S_5 and S_6 are OFF. No parallel inductor is implemented. The WPT system operates as the original LLC WPT system. Set f_{sw} to f_{r1} and the circuit gain M_{g1} is 1. Since the secondary side leakage inductance is compensated, there would be no voltage drop after the receiver coil to the load.

Mode 2: Turn both S_5 and S_6 to the ON state. L_p would be parallel connected to the transmitter coil. Aforementioned, the voltage gain would not be an ideal value if the load and Q_e stay at a high level which penetrates the unnecessary reactive power into the WPT system. Therefore, f_{sw} remains at f_{r1}. The circuit gain M_{gp} would be higher than unity in mode 1 because the parallel inductor declines the circuit impedance.

C. ZVS

The ZVS principle of mode 1 and mode 2 is very similar. System ON ZVS could be realized by the conduction of the inverter switches body diodes. Before the switches turn ON, I_r will flow through the switches' body diodes and clamp the switches' voltage at the diode forward voltage level, which is usually comparatively low. The reverse conduction would last after the switching is completed. The switching loss remains as the diode loss.

In mode 1, the ZVS frequency area is from the vicinity of the circuit resonant frequency $f_{r0} = 1/2\pi\sqrt{(L_{r1} + L_m)C_{r1}}$ with the FHA. At no load or light load conditions, this could be accurate but still should be tuned after the plotting of the gain-frequency curve. In this paper, $f_{sw} = f_{r1}$ which is far from f_{r0} at most times.

$t_0 - t_1$: S_1, S_4 are ON whereas S_2, S_3 are OFF. V_{in} supplies the resonant tank through S_1, S_4 thus I_r increases to the positive direction. The current waveform could be treated as the superposition of the Tx magnetizing reactance current and the load combined resonant current.

$t_1 - t_2$: this is the fall time of active switches. Since the circuit is operating at f_{r1}, the Rx side reflected current is zero. Hence, I_r equals I_m. V_{ds1}, V_{ds4} are declining to zero while V_{ds2}, V_{ds3} climbs. The drop of S_1 and S_4 conducting capacity penetrates a portion value of I_r to the reverse diode of S_2, S_3. Hence, the inverse direction of S_2 voltage current prevents the active switch from consuming power from V_{in}. Instead, the integral of reverse diode forward voltage V_{sd} and I_{s2} contributes to the switching ON energy loss. Due to the comparatively low value of V_{sd} to V_{in}, ZVS is achieved. The

sum of switching ON loss $P_{s.ON}$ could be accessed by (30).

$$P_{s.ON} = 4P_{s2.ON} = 4f_{r1}\int_{t_1}^{t_2} V_{sd}I_{s2}dt \tag{30}$$

$t_2 - t_3$: the symmetrical process of $t_0 - t_1$. The only difference is the opposite flowing direction of I_r due to the complementary conducting switches of the H-bridge.

$t_3 - t_4$: S_2, S_3 are turning OFF and the corresponding conducting current lessens rapidly. Identical to $t_1 - t_2$, S_1, S_4 conduct as ZVS while S_2, S_3 experience the hard switching. The switching OFF loss $P_{s.OFF}$ could be estimated as (31).

$$P_{s.OFF} = 4P_{s2.OFF} = -4f_{r1}\int_{t_3}^{t_4} V_{in}I_r dt \tag{31}$$

In mode 2, L_p decreases Z_{in} so that the resonant frequency becomes larger. The main benefit is a greater M_{gp} so that the WPT system can transfer a higher voltage level with a constant f_{sw}. The control strategy becomes simple. The prevention of mode 2 slipping to the non-ZVS area is the only concern.

D. LOSS ANALYSIS

Losses could be specified as conduction loss, switching loss and magnetic core loss. Conduction loss could be estimated by the Ohm's law. The core loss P_{core} comprises eddy current loss P_e, hysteresis loss P_h, and residual loss P_r denoted as $tan\delta/\mu_i$ [36]. μ_i the core reactance relevant permeability and $tan\delta = R_{loss}/\omega L$ presents the ratio of equivalent core loss equivalent resistance R_{loss} to the coil reactance ωL. P_e contributes little as the large core resistivity. Theoretically, P_r is proportional to P_h and be linear to B_m^2. In practical cases, Steinmetz's equation $P_{core} = k_{core}B_m^a f^b V_e$ is effective in estimating the core power loss in which k_{core}, a and b are the physical related constant. The amplitude of magnetic field density dominates in the ferrite core when compared with the operating frequency. (32, 33) illustrate the calculation method and the advantage of the increasing modulation frequency characteristics, which keep B_m within the linear range.

$\hat{I}_m$, $\hat{I}_{tc}$ and $\hat{B}_m$ are the circuit maximum magnetizing current, transmitter coil current and magnetic field density in ferrite, respectively. l_e, μ_e and μ_0 are the equivalent magnetic loop length, relative permeability and the magnetic permeability of free space.

$$\hat{B}_{m1} = \frac{2\mu_0\mu_e I_{tc1}N_1}{l_e} \tag{32}$$

$$\hat{B}_{m2} = \frac{2\mu_0\mu_e I_{tc2}N_1}{l_e} \tag{33}$$

The switching OFF loss is considered by the integration of the switching current and voltage. In Mode 1, the conventional LLC WPT inverter switches cut-off current $I_{r1.OFF}$ equals to the amplitude of the magnetizing current $\hat{I}_m$ while in mode2, the switching OFF current $I_{r2.OFF}$ consists of the peak value of the magnetizing current and parallel inductor current:

$$I_{r1.OFF} = \hat{I}_{m1} = 2M_g V_{ge}/j\omega_1 L_m \tag{34}$$

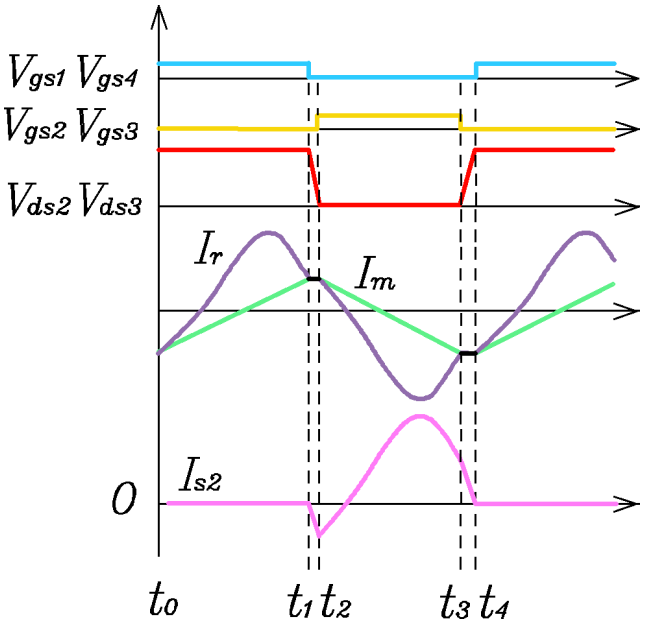

FIGURE 8. The active switch's body diode conducts when turning ON.

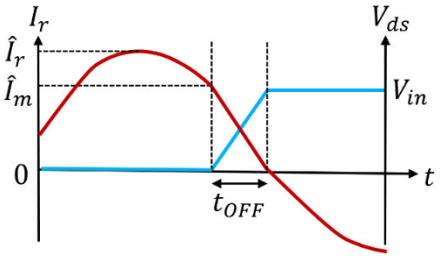

FIGURE 9. Active switch switching OFF status.

$$I_{r2.OFF} = \hat{I}_{m2} + \hat{I}_{p1} = \frac{2M_{gp}V_{ge}}{j\omega_1 L_m} + \frac{2\left[I_{tc2}j\omega_1 L_{r1} + M_{gp}V_{ge}\right]}{j\omega_1 L_p} \tag{35}$$

$$P_{s.OFF} = 4P_{s2.OFF} = 4f_{r1}\int V_{in}I_{r.OFF}dt \tag{36}$$

According to [35], the drain-source current decays linearly when the voltage climbs. Integrating the product of V_{ds} and I_r will get the switching loss at OFF progress. Therefore, shows as Fig.9, the switching loss of the inverter switch could be estimated by:

$$P_{sw.loss} = 4(\omega_1 t_{OFF}V_{in}I_{r.OFF}/12\pi) = \omega_1 t_{OFF}V_{in}I_{r.OFF}/3\pi \tag{37}$$

IV. SIMULATION STUDY

Simulations and the circuit design framework are illustrated in this section. As depicted in Fig.10, the magnetic design would be prior to the electric circuit design. Higher mutual inductance saves the coil copper and device volume due to the smaller magnetizing current. FEA provides the preliminary inductance distribution of Tx, Rx self-inductance and the

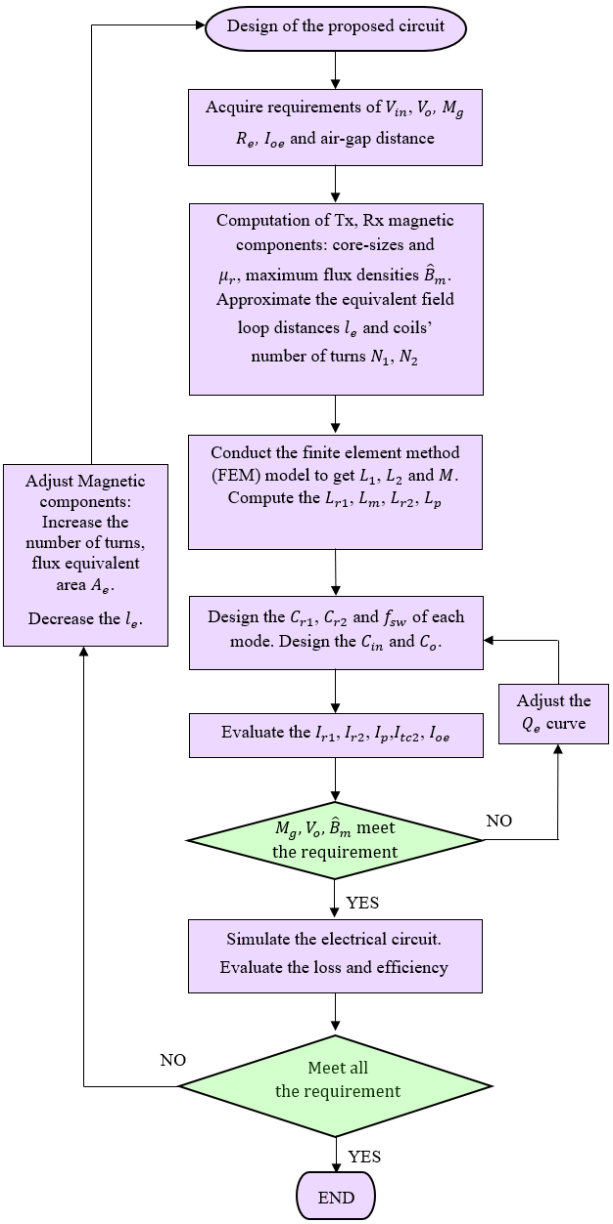

FIGURE 10. Mode 1 simulation results with 43V output voltage.

coupling coefficient. Operation frequency could be adjusted by the resonant capacitors. Aforementioned, the Q_e is related to the gain profile and the preliminary design could be fail. Thus, the comprehension workout could be conducted for several times. This simulation study exhibits the design procedure with details.

A. MAGNETIC COMPONENT DESIGN

A vertical flux magnetic coil layout applies in the Tx and Rx in this case. An important reason is the planar spiral coil design could be slim and compact and also mitigates the orientational misalignment for practical applications. Tx and Rx inductance and coupling-coefficient could be accessed by finite element analysis (FEM). Fig.11 shows the FEM simulation model of the Tx and Rx coils conducted by the ANSYS Maxwell. The symmetrical Tx and Rx specification reveals in Table 1. High relative permeability ferrite is applied to increase the coil inductance. Turns ratio of Tx and Rx is 16:16.

TABLE 1. Magnetic simulation parameters.

TX and Rx dimension (mm)	135×130×23.4
ferrite pad dimension (mm)	135×130×20
ferrite relative permeability	3300
Core-coil alignment	Centre alignment
Wire diameter (mm)	3.4
Wire number of turns	16
Coil radius (mm)	81
Air-gap distance (mm)	12
Self-inductance (μH)	31.61
Tx coil leakage inductance (μH)	7.40
Magnetizing inductance (μH)	24.21
Rx leakage inductance (μH)	7.41
Coupling coefficient	0.76

TABLE 2. Proposed circuit simulation parameters.

Input voltage (V)	45
f_{rl} (kHz)	103.4
C_{rl} and C_{r2} (nF)	320
L_p (μH)	24
Turns ratio	1
M_g	1
M_{gp}	1.2
Load resistance (Ω)	8.2
Resonant capacitor equivalent series resistance (mΩ)	60
MOSFET conducting resistance (mΩ)	19
Coil resistance (mΩ)	60
L_p resistance (mΩ)	2

B. CIRCUIT DESIGN

To cater the vehicular and portable electronic device application, the switching frequency was selected at kilo Hertz range. The capacitances of C_{r1} and C_{r2} were 320μH to make the resonant frequency f_{r1} at 103.4kHz. Therefore, the M_g of mode 1 should be 1 when f_{sw} was set at f_{r1}. Tx and Rx number-of-turns were identical; thus, the turns ratio was 1. Considering the practical implementation that an ultrafast diode would be chosen as Rx side rectifier, the diode forward voltage drop was rated at 1.5V. Derived from (25-27), a 24μH L_p was parallel connected to the Tx coil.

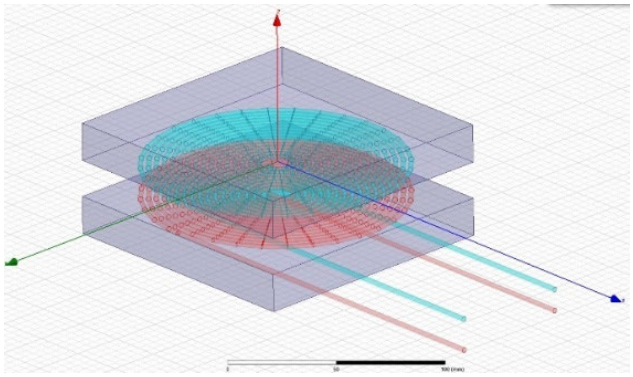

FIGURE 11. FEM simulation of the Tx and Rx self-inductances and k.

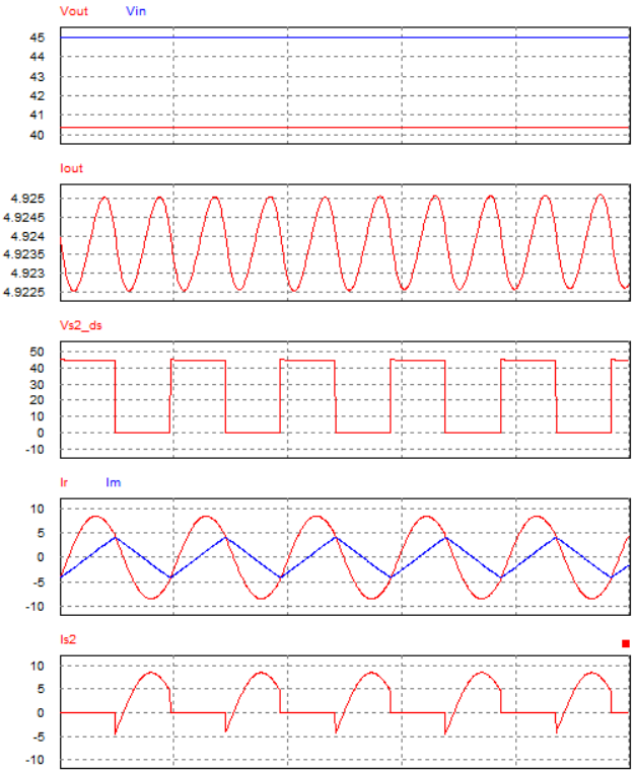

FIGURE 12. Mode 1 simulation results with 43V output voltage.

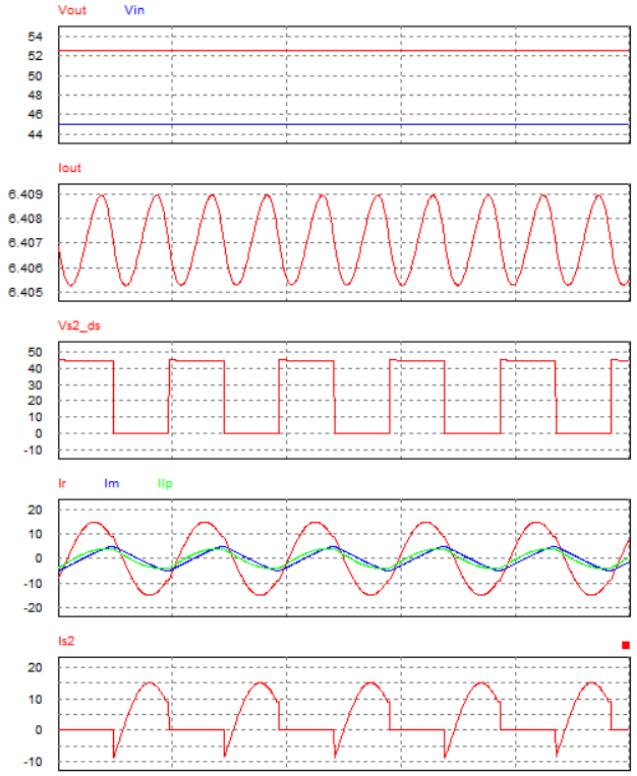

FIGURE 13. Mode 2 simulation results with 52.5V output voltage.

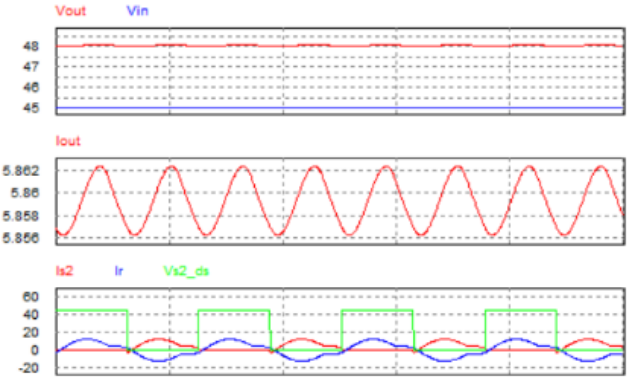

FIGURE 14. Conventional LLC frequency modulation limitation.

C. SIMULATION RESULTS

For the 45V V_{in} and 8.2 Ω load condition, Fig.12 depicts the mode 1 operation characteristics. The output voltage V_{out} equals 40.3V which was 4.7V lower V_{in}. 3V voltage drop came from the rectifier diode. With regardless to it, the under-voltage performance stated −3.8% of the gain error whereas the ripple could be neglected. Output current I_{out} was 4.9A. At the moment when S_2 was ON, I_r changed the flowing path from S_1 to the reversed diode of S_2 so that the corresponding ZVS was realized. Fig.13 demonstrates the mode 2 operation profile. V_{out} has been step-up to 52.5V that is 30% increment of mode1. At the same time, output power rose from 197.5W to 336.1W. Similar to mode1, the output current ripple also kept within a very fine interval and ZVS was achieved. The system efficiency was 93.4% at mode 2.

D. COMPARISON WORK ON SIMULATIONS

The proposed topology performs to expand the LLC WPT voltage gain as the result of simulation. In mode 1, Q_e is 0.59, which delivers a sharp gain attenuation versus frequency. Conventional LLC WPT, in desire of higher output power, decreasing the f_{sw} could reach the maximum V_{out}. It is 48.0V shown in Fig.13 whereas the coil current I_r is 8.0A, $\hat{I}_r$ = 12.2A. However, mode 2 demonstrates that even the output power and voltage V_{out} are higher, the coil current of I_m

TABLE 3. Comparison of proposed switched inductor LLC circuit and frequency modulation LLC method.

	Mode 2	Frequency modulated LLC
f_{sw} (kHz)	103.4	79.2
Output power (W)	336.6	281.0
Output voltage V_{out}	52.5	48.0
Circuit gain M_g	1.2	1.1
Switched current I_r (A)	10.6	8.0
Coil current (A)	8.2	8.0
Peak magnetizing current (A)	11.8	12.2
Efficiency (%)	93.4	90.6

maintains at 8.2A, and $\hat{I}_m$ remains at 11.8A. This results in higher operational efficiency.

V. EXPERIMENTAL RESULTS AND BENCHMARKING

A. IMPLEMENTATION

To verify the concept of the inductor-aid step-up LLC WPT system and compare the performances to the conventional LLC, a 300W prototype has been conducted. The hardware setup referred to the simulation parameters was designed as Fig.15. The marking number 1 is DC power supply, 2 is the proposed converter, 3 is the Tx and Rx magnetic components, 4 is the Rx side compensation tank and rectifier, 5 is an electronic load which was set as resistance, 6 is an oscilloscope, 7 is the differential voltage probe and 8 is the current transducer. The specifications are exhibited in TABLE 4. Magnetic components such as the Tx, Rx self-inductances and k matched the simulation results in the last subsection. For high-frequency operation, polypropylene capacitor has been deployed as resonant capacitors. Core and coil were packaged into the acrylic boxes to merge the magnetic modules that mock the real application scenario. Since mode 1 operation is the conventional LLC circuit, the comparison would be established on the same converter.

B. EXPERIMENTAL RESULTS

Results of about 300W power conversion depicted in Fig.16. V_{s2g} represents the gate signal of S_2 while V_{s2} stands for the MOSFET drain-source voltage. In both figures, I_r was positive current when S_2 turned ON. This ensures the ZVS switching. The converter input voltage was 45V, the resistance load was 8.2Ω and the switching frequency was set at 103.3kHz to ensure the circuit gain is 1. In Fig.16 (a), The mode 1 output voltage of load V_o is 43V while I_r is 6.18A. The voltage drop from 45V to 41V could be explained as the rectifier diodes and loop resistance voltage drop. Obviously, ZVS has been achieved and the ripple of the output voltage is about 3V. Output power is 205W with 96.2% efficiency. In mode 2, L_p has been deployed and $V_o = 50.4$V. The circuit efficiency is 90% with the 310W output power. The output voltage level is just 4% lower than the simulation and the ripple is revealed

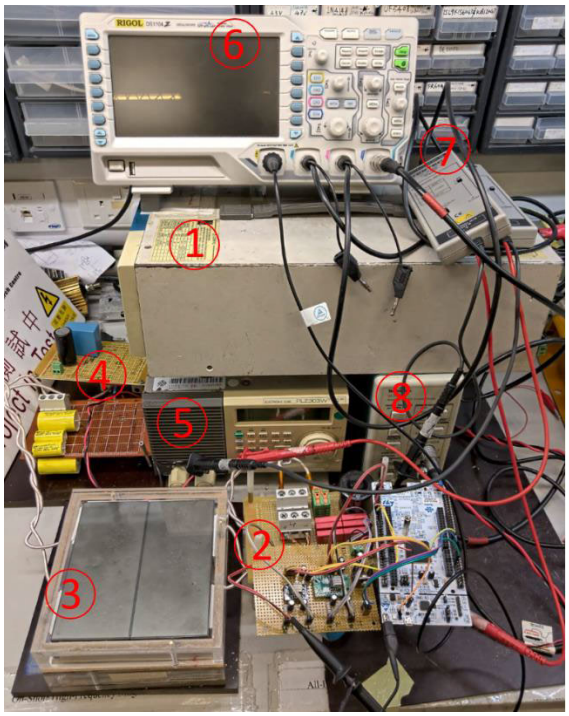

FIGURE 15. Picture of the 300W experimental prototype.

TABLE 4. Experimental converter parameters.

Packaged TX and Rx dimension (mm)	147×142×32
ferrite model	PC95SP135X65X20
Ferrite relative permeability	3300
Airgap (mm)	12
N_1:N_2	16:16
Self-inductance of Tx (μH)	30.2
Self-inductance of Rx (μH)	30
Mutual inductance (μH)	23
Coupling coefficient k	0.76
Tx, Rx resonant capacitance (nF)	330
Resonant frequency f_{r1} (kHz)	103
Switching frequency f_{sw} (kHz)	103.3
L_p model	B65733A0000R087
L_p value (μH)	25.6
Mode 2 step-up ratio at f_{r1}	1.2
Active switch model	IRFP250PBF
300W efficiency η	90%

at 6.0%. Considering the voltage drop of diodes, the mode2 gain should be 1.18. Using the conventional circuit and loss analysis, diodes contribute about 19W power loss, conduction

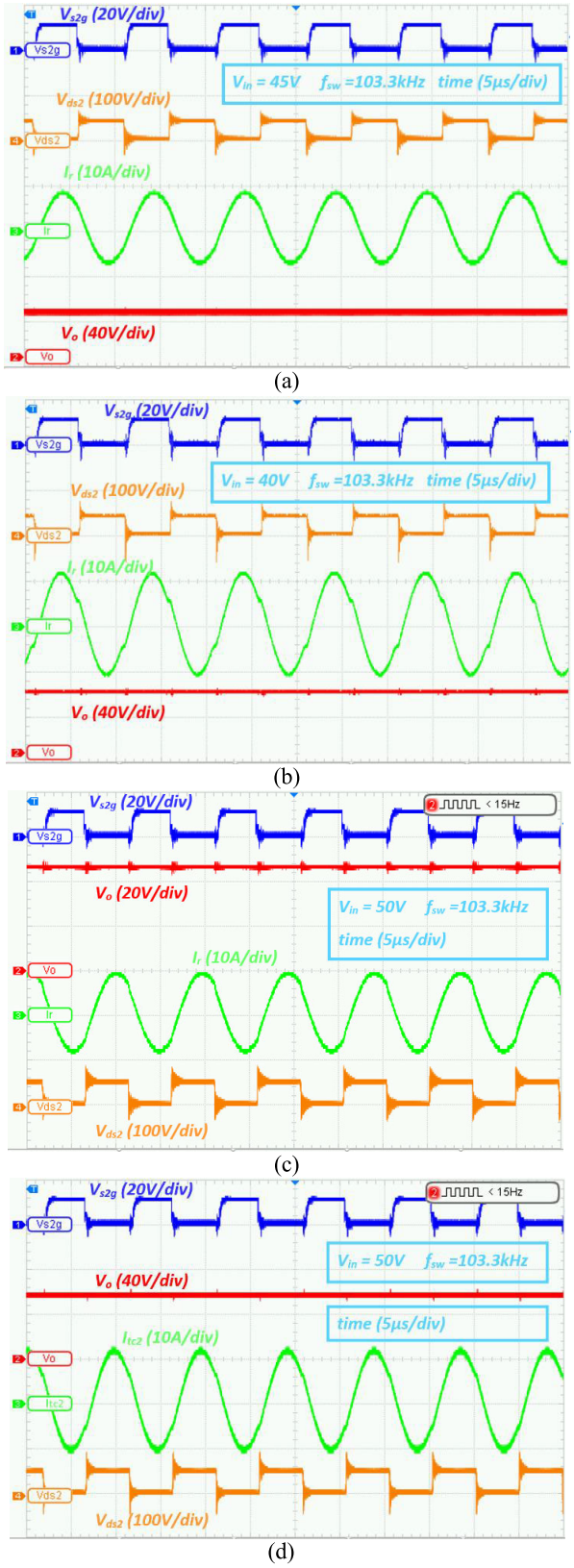

FIGURE 16. Experimental waveforms of the proposed circuit: (a) Mode 1 operation and V_o = 41V (R_o = 8.2 Ω), (b) Mode 2 operation and V_o = 50.4V (R_o = 8.2 Ω). (c) V_{in} = 50V, Mode 1 operation and V_o = 46V (R_o = 10 Ω), (d) V_{in} = 50V, Mode 2 operation and V_o = 56V (R_o = 10 Ω).

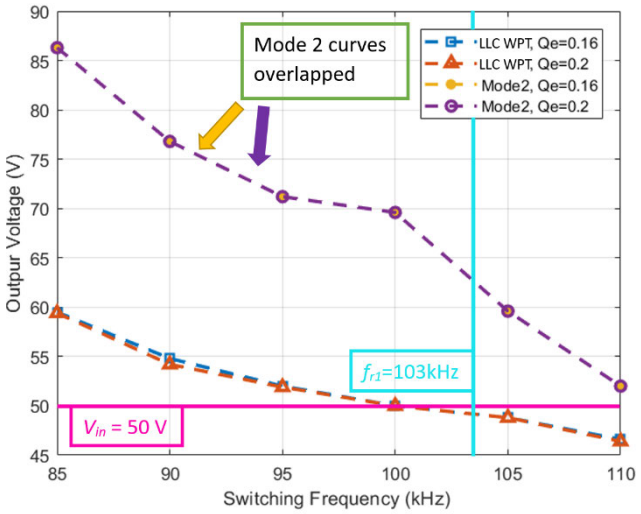

FIGURE 17. Output voltage experimental results comparison of the conventional LLC WPT frequency modulation and the proposed inductor-aid step-up method.

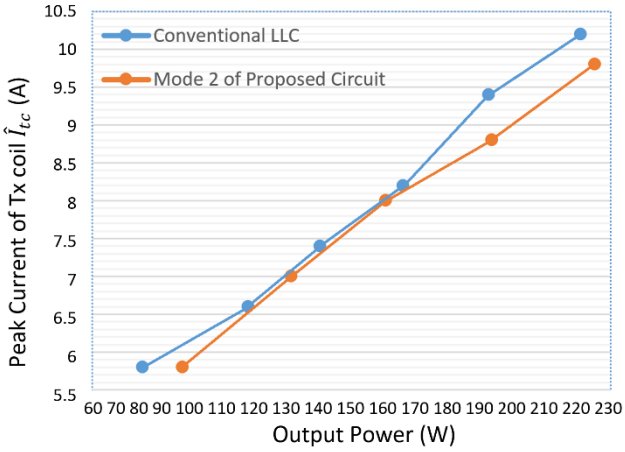

FIGURE 18. Tx coil current experimental results comparison of the conventional LLC WPT system frequency modulation and the proposed inductor-aid step-up method.

loss of active switches, coil and cables is around 6W, and 9W is the magnetic components losses, including the ferrite of Tx, Rx and L_p.

In Fig.16 (c) and (d), V_{in} has been increased to 50V whereas the load is 10Ω. Mode 1 performed the 46V at the load side and transmitted 211W output power with 92% efficiency. Mode 2 step-up the output voltage at 56V and transferred 313W output power with 89% efficiency. The step-up voltage gain ratio is 20%.

The comparison of the conventional LLC and the proposed circuit has been made showed as Fig.17 and Fig. 18. According to the fit curves of Fig. 17, the proposed inductor-aid step-up LLC in the WPT system is capable of transferring a higher voltage level at the load side even when the conventional LLC applied the −17% frequency modulation. The merit of

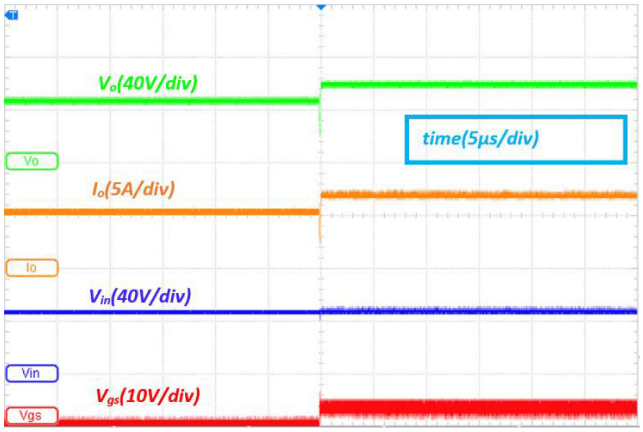

FIGURE 19. Experimental waveforms of the proposed circuit: From top to below, CH1: output voltage; CH2: output current; CH3: input voltage; CH4: gate-source signal value of S_5, S_6.

L_p-aid constant f_{sw} operation is the stable performances of the ferrite and resonant tanks on both sides. Fig. 18 reveals that the proposed circuit requires less $\hat{I}_r$ in the Tx coil when it delivers the same output power. This means the WPT system of the proposed circuit would have a higher magnetic flux density redundancy.

Figure. 19 indicates the switching ON process of S_5 and S_6, which conduct to boost up the output voltage. Benefits from the primary control, zero-current detection is unnecessary to outset the higher voltage power transmission. Switching OFF the system and restarting with parallel inductor ON was realized within 1ms. The voltage drop of less than 0.3V rms value across S_5 and S_6 at full load condition is presented in Fig. 20 (a) and (b), of which the WPT circuit was triggered from mode 1 to mode 2, which confirms the theory analysis.

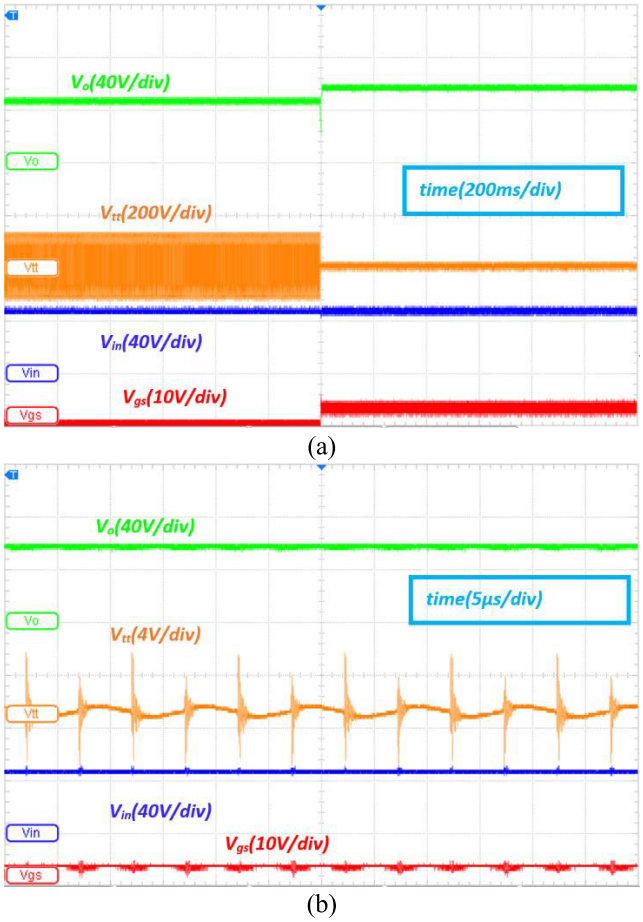

FIGURE 20. Experimental waveforms of the proposed circuit when turning from mode1 to mode 2: From top to below, CH1: output voltage; CH2: voltage between transistors S_5, S_6; CH3: input voltage; CH4: gate-source signal value of S_5, S_6. (a) 200ms/div (b) 5μs/div.

C. BENCHMARKING

In the WPT system, the proposed circuit provides a straightforward method to step up the output voltage much higher than the conventional frequency control, let alone the constant frequency operation has no mismatch concern over the resonant tanks. When compared with the conventional boost converter placed before or after the overall WPT system, adding two active switches and one inductor in Tx side could be compact and convenient to implement. Since the boost converter raises the higher voltage requirement of the H-bridge active switches if the boost converter is installed before the H-bridge. The higher input voltage would also increase the As in the case of the boost converter at Rx side, it brings the drawbacks of bulky and redundancy, due to the Rx sides would have the corresponding charging regulation converter in the practical battery charging applications. In addition, the control method as the solid-state relay of L_p is not complicated to step up the output voltage. Practically, the proposed would be fitter to upgrade the existing constant frequency operation constant output voltage LLC WPT system facility and standard due to the explicit layout. A larger step-up ratio benefits the multi-frequency LLC WPT system and enlarges the applications. The smaller Tx coil current ensures the normal operation of magnetic components as the old method. What is more, it could be realized without any extra fore converter and the mass modification of the inverter switch.

VI. CONCLUSION

In this paper, an inductor-aid step-up LLC WPT system has been proposed. Without any extra hardware installation on the secondary side, this method extends the LLC WPT applications output voltage from constant value to multi-level, such as the battery slow-charge and fast-charge applications of vehicles and portable electronic devices. Mode 1 is the conventional LLC WPT system, whilst Mode 2 delivers a higher output voltage by turning ON the parallel inductor. Adding the extra inductors and straightforward control on Tx side without any modifications on Rx side, existing WPT systems which require higher capacity, could be benefited from this easy-refit feature. Illustrate comprehensively, LLC WPT fundamental which is the basis of steady-state illustration, was introduced. The voltage gain characteristics and operation

principle have been investigated with circuit analysis and frequency response. This paper also provides the structural design flow chart and the comprehensive design procedure from a simulation study to the experiment implementation. A 90% efficiency 382W prototype has been constructed to verify the circuit characteristics and to compare with the conventional frequency modulation method. Results proved that the proposed method has a higher step-up ratio and releases the magnetic ferrite flux density stress in case saturation and overheating occur. The drawback is when the higher step-up ratio is desired, a smaller L_p is required. It leads to the adverse condition in high magnetic flux in $L_{p,}$ and the conversion range is then limited. The potential of the topology is the selected multiple parallel inductors connection to the transmitter coils to build a flexible and multi-output voltage level WPT system.

REFERENCES

[1] V. Cirimele, M. Diana, F. Freschi, and M. Mitolo, "Inductive power transfer for automotive applications: State-of-the-art and future trends," *IEEE Trans. Ind. Appl.*, vol. 54, pp. 4069–4079, Sep./Oct. 2018, doi: 10.1109/TIA.2018.2836098.

[2] D. van Wageningen and T. Staring, "The Qi wireless power standard," in *Proc. 14th Int. Power Electron. Motion Control Conf. (EPE-PEMC)*, Sep. 2010, pp. S15-25–S15-32, doi: 10.1109/EPEPEMC.2010.5606673.

[3] S. Li and C. C. Mi, "Wireless power transfer for electric vehicle applications," *IEEE J. Emerg. Sel. Topics Power Electron.*, vol. 3, no. 1, pp. 4–17, Mar. 2015, doi: 10.1109/JESTPE.2014.2319453.

[4] X. Xin, D. R. Jackson, and J. Chen, "Wireless power transfer along oil pipe using ferrite materials," *IEEE Trans. Magn.*, vol. 53, no. 3, pp. 1–5, Mar. 2017, doi: 10.1109/TMAG.2016.2626254.

[5] K. Agarwal, R. Jegadeesan, Y. Guo, and N. Thakor, "Wireless power transfer strategies for implantable bioelectronics," *IEEE Rev. Biomed. Eng.*, vol. 10, pp. 136–161, 2017, doi: 10.1109/RBME.2017.2683520.

[6] C. Zhang, D. Lin, and S. Y. R. Hui, "Ball-joint wireless power transfer systems," *IEEE Trans. Power Electron.*, vol. 33, no. 1, pp. 65–72, Jan. 2018, doi: 10.1109/TPEL.2017.2700898.

[7] G. L. Barbruni, P. M. Ros, D. Demarchi, S. Carrara, and D. Ghezzi, "Miniaturised wireless power transfer systems for neurostimulation: A review," *IEEE Trans. Biomed. Circuits Syst.*, vol. 14, no. 6, pp. 1160–1178, Dec. 2020, doi: 10.1109/TBCAS.2020.3038599.

[8] H.-J. Kim, H. Hirayama, S. Kim, K. J. Han, R. Zhang, and J.-W. Choi, "Review of near-field wireless power and communication for biomedical applications," *IEEE Access*, vol. 5, pp. 21264–21285, 2017, doi: 10.1109/ACCESS.2017.2757267.

[9] X. Lu, P. Wang, D. Niyato, D. I. Kim, and Z. Han, "Wireless charging technologies: Fundamentals, standards, and network applications," *IEEE Commun. Surveys Tuts.*, vol. 18, no. 2, pp. 1413–1452, 2nd Quart., 2016, doi: 10.1109/COMST.2015.2499783.

[10] V. Shevchenko, S. Member, O. Husev, and S. Member, "Compensation topologies in IPT systems: Standards, requirements, classification, analysis, comparison and application," *IEEE Access*, vol. 7, pp. 120559–120580, 2019, doi: 10.1109/ACCESS.2019.2937891.

[11] A. Ahmad, M. S. Alam, and R. Chabaan, "A comprehensive review of wireless charging technologies for electric vehicles," *IEEE Trans. Transport. Electrific.*, vol. 4, no. 1, pp. 38–63, Mar. 2018, doi: 10.1109/TTE.2017.2771619.

[12] C.-S. Wang, O. H. Stielau, and G. A. Covic, "Design considerations for a contactless electric vehicle battery charger," *IEEE Trans. Ind. Electron.*, vol. 52, no. 5, pp. 1308–1314, Oct. 2005, doi: 10.1109/TIE.2005.855672.

[13] X. Tan and X. Ruan, "Equivalence relations of resonant tanks: A new perspective for selection and design of resonant converters," *IEEE Trans. Ind. Electron.*, vol. 63, no. 4, pp. 2111–2123, Apr. 2016, doi: 10.1109/TIE.2015.2506151.

[14] G. Ivensky, S. Bronshtein, and A. Abramovitz, "Approximate analysis of resonant LLC DC-DC converter," *IEEE Trans. Power Electron.*, vol. 26, no. 11, pp. 3274–3284, Nov. 2011, doi: 10.1109/TPEL.2011.2142009.

[15] M. Noah, K. Umetani, J. Imaoka, and M. Yamamoto, "Lagrangian dynamics model and practical implementation of an integrated transformer in multi-phase LLC resonant converter," *IET Power Electron.*, vol. 11, no. 2, pp. 339–347, Feb. 2018.

[16] J. Liu, J. Zhang, T. Q. Zheng, and J. Yang, "A modified gain model and the corresponding design method for an LLC resonant converter," *IEEE Trans. Power Electron.*, vol. 32, no. 9, pp. 6716–6727, Sep. 2017.

[17] J. Niu, Y. Tong, Q. Ding, X. Wu, X. Xin, and X. Wang, "Time domain simplified equations and its iterative calculation model for LLC resonant converter," *IEEE Access*, vol. 8, pp. 151195–151207, 2020, doi: 10.1109/ACCESS.2020.3016975.

[18] Y. Wei, Q. Luo, S. Chen, P. Sun, and N. Altin, "Comparison among different analysis methodologies for LLC resonant converter," *IET Power Electron.*, vol. 12, no. 9, pp. 2236–2244, Aug. 2019, doi: 10.1049/iet-pel.2019.0027.

[19] C. Shen, H. Zhong, Y. Zhang, Y. Tang, and Y. Zhang, "Design method of 6-element boundary gain for LLC resonant converter of electric vehicle," *IEEE Access*, vol. 8, pp. 183090–183100, 2020, doi: 10.1109/ACCESS.2020.3028941.

[20] J. Ni, J. Hu, and C. Xiang, "Control-configured-vehicle design and implementation on an X-by-wire electric vehicle," *IEEE Trans. Veh. Technol.*, vol. 67, no. 5, pp. 3755–3766, May 2018.

[21] K. L. J. Kan, Y. C. Fong, I. S. Chuen, H. K. T. Tsang, H. F. Ho, X. D. Xue, Y. L. Fan, and K. W. E. Cheng, "Electric waterjet thruster vessel development—Concept, charger, and battery monitoring," in *Proc. 8th Int. Conf. Power Electron. Syst. Appl. (PESA)*, Dec. 2020, pp. 1–7, doi: 10.1109/PESA50370.2020.9344015.

[22] H. Wang, S. Dusmez, and A. Khaligh, "Design and analysis of a full-bridge LLC-based PEV charger optimized for wide battery voltage range," *IEEE Trans. Veh. Technol.*, vol. 63, no. 4, pp. 1603–1613, May 2014, doi: 10.1109/TVT.2013.2288772.

[23] H.-P. Park and J.-H. Jung, "Power stage and feedback loop design for LLC resonant converter in high-switching-frequency operation," *IEEE Trans. Power Electron.*, vol. 32, no. 10, pp. 7770–7782, Oct. 2017, doi: 10.1109/TPEL.2016.2635261.

[24] G. Zhang, J. Zeng, S. Shenglong Yu, W. Xiao, B. Zhang, S.-Z. Chen, and Y. Zhang, "Control design and performance analysis of a double-switched LLC resonant rectifier for unity power factor and soft-switching," *IEEE Access*, vol. 8, pp. 44511–44521, 2020, doi: 10.1109/ACCESS.2020.2978030.

[25] C. Liu, H. Liu, G. Cai, S. Cui, H. Liu, and H. Yao, "Novel hybrid LLC resonant and DAB linear DC-DC converter: Average model and experimental verification," *IEEE Trans. Ind. Electron.*, vol. 64, no. 9, pp. 6970–6978, Sep. 2017, doi: 10.1109/TIE.2017.2682784.

[26] H. Xu, Z. Yin, Y. Zhao, and Y. Huang, "Accurate design of high-efficiency LLC resonant converter with wide output voltage," *IEEE Access*, vol. 5, pp. 26653–26665, 2017, doi: 10.1109/ACCESS.2017.2757764.

[27] J. H. Kim, "Development of 1-MW inductive power transfer system for a high-speed train," *IEEE Trans. Ind. Electron.*, vol. 62, no. 10, pp. 6242–6250, Oct. 2015, doi: 10.1109/TIE.2015.2417122.

[28] H. Wang, K. W. E. Cheng, X. Li, and J. Hu, "A special magnetic coupler structure for three-coil wireless power transfer: Analysis, design, and experimental verification," *IEEE Trans. Magn.*, vol. 57, no. 11, pp. 1–8, Nov. 2021.

[29] L. Meng, K. W. E. Cheng, and K. W. Chan, "Systematic approach to high-power and energy-efficient industrial induction cooker system: Circuit design, control strategy, and prototype evaluation," *IEEE Trans. Power Electron.*, vol. 26, no. 12, pp. 3754–3765, Dec. 2011.

[30] L. Meng and K. W. E. Cheng, "Wireless power transfer technology for electric iron based on multi-coils induction heating design," *IET Power Electron.*, vol. 12, no. 10, pp. 2566–2577, Aug. 2019.

[31] C. Wang, C. Zhu, G. Wei, J. Feng, J. Jiang, and R. Lu, "Design of compact three-phase receiver for meander-type dynamic wireless power transfer system," *IEEE Trans. Power Electron.*, vol. 35, no. 7, pp. 6854–6866, Jul. 2020, doi: 10.1109/TPEL.2019.2955203.

[32] J. Shin, "Design and implementation of shaped magnetic-resonance-based wireless power transfer system for roadway-powered moving electric vehicles," *IEEE Trans. Ind. Electron.*, vol. 61, no. 3, pp. 1179–1192, Apr. 2014, doi: 10.1109/TIE.2013.2258294.

[33] S. Gao and Z. Zhao, "Magnetic integrated LLC resonant converter based on independent inductance winding," *IEEE Access*, vol. 9, pp. 660–672, 2021, doi: 10.1109/ACCESS.2020.3046616.

[34] Y. Wei, Q. Luo, and A. Mantooth, "Comprehensive analysis and design of LLC resonant converter with magnetic control," *CPSS Trans. Power Electron. Appl.*, vol. 4, no. 4, pp. 265–275, Dec. 2019, doi: 10.24295/CPSST-PEA.2019.00025.
[35] A. Ayachit and M. K. Kazimierczuk, "Averaged small-signal model of PWM DC-DC converters in CCM including switching power loss," *IEEE Trans. Circuits Syst. II, Exp. Briefs*, vol. 66, no. 2, pp. 262–266, Feb. 2019, doi: 10.1109/TCSII.2018.2848623.
[36] (Dec. 2015). *Soft Ferrites Products Guide*. Accessed: Sep. 5, 2021. [Online]. Available: http://www.hitachi-metals.co.jp/e/products/elec/tel/pdf/hj-b3-e.pdf#page=40

KIN LUNG JERRY KAN received the B.Eng. degree in electrical engineering and its automation from the South China University of Technology, Guangzhou, China, in 2017, and the M.Sc. degree in electrical engineering from The Hong Kong Polytechnic University, Hong Kong, in 2018, where he is currently pursuing the Ph.D. degree with the Department of Electrical Engineering.

He joined the Department of Electrical Engineering, The Hong Kong Polytechnic University, as a Research Assistant, in 2018. His research interests include wireless power transfer, dc–dc power converters, and marine electrification.

KA WAI ERIC CHENG (Fellow, IEEE) received the B.Sc. and Ph.D. degrees from the University of Bath, Bath, U.K., in 1987 and 1990, respectively.

Before joining The Hong Kong Polytechnic University, Hong Kong, in 1997, he was with Lucas Aerospace, London, U.K., as a Principal Engineer. He is currently a Professor and the Director of the Power Electronics Research Centre, Department of Electrical Engineering, Faculty of Engineering, The Hong Kong Polytechnic University. He has authored or coauthored more than 500 articles and seven books. His research interests include all aspects of power electronics, motor drives, electromagnetic interference, electric vehicles, battery management, and energy saving. He was a recipient of the Institution of Electrical Engineers Sebastian Z. De Ferranti Premium Award, in 1995; the Outstanding Consultancy Award, in 2000; the Faculty Merit Award for Best Teaching from The Hong Kong Polytechnic University, in 2003; the Faculty Engineering Industrial and Engineering Services Grant Achievement Award, in 2006; the Brussels Innova Energy Gold Medal with Mention, in 2007; the Consumer Product Design Award, in 2008; the Electric Vehicle Team Merit Award of the Faculty, in 2009; the Eco Star Award, in 2012; the Gold Prize at Seoul International Invention Fair, in 2015; the iCAN Gold Medal at Canada for contribution in active suspension, in 2016; the Gold Award of Hong Kong Innovation and Technology for contribution in body integrated super capacitor for vehicles, in 2017; and the Geneva Invention Expo Silver Medal for contribution in e-Antilock braking systems, in 2021.